Correspondence

Elastographic Axial Resolution Criteria: An Experimental Study

S. Kaisar Alam, *Senior Member, IEEE*,
Jonathan Ophir, *Member, IEEE*,
and Tomy Varghese, *Member, IEEE*

***Abstract*—In elastography, window size has been typically used synonymously with resolution. Strain is estimated by computing the gradient of the displacement estimates, which have a direct dependence on the window size. However, the resolution is also dependent on the separation between these windows. The intricate relationship between the window size, window shift, and resolution has not previously been explored. In this article, we perform a controlled simulation experiment to evaluate the relationship among elastographic axial resolution, window size, and window shift. We conclude that the axial resolution can be expressed as a bilinear function of window size and window shift, the latter having a much larger weight.**

I. Introduction

Resolution is one of the primary image parameters in any imaging modality. In many imaging modalities, the resolution depends only on the size of the data window. However, in an elastographic system, axial resolution is determined by a complex interaction between the data window size and the overlap between successive windows. In elastography [1], strain is generally estimated from the gradient of displacement estimates. The displacements between the pre- and postcompression echo signals are estimated at various depths by shifting the data windows. This displacement is a monotonically nondecreasing function of depth; as a result, it is rarely constant within a data window. When displacement varies, correlation function maxima generally correspond to the mean of the displacements within the data window [2]. We can change resolution by changing either the sampling or the averaging. Increasing the window size (T) increases averaging, reducing the effect of motion of an individual scatterer. Changing the window shift (Δt), on the other hand, alters the sampling. A higher sampling assists in the detection of sharp changes. Thus, changes in T affect the statistics, and changes in Δt affect the sampling of the displacement estimates. As a result, a change in either T or Δt affects the axial resolution. In this work, we postulate that the resolution can be expressed as a function of the window size and window shift [$R = R(T, \Delta t)$].

In the past, we have used the window size (at a fixed percentage of window overlaps) synonymously with the resolution [3]. Cespedés [4] investigated elastographic resolution using the axial and lateral step response approaches without actually attempting to define resolution. The step response demonstrated a strong dependence on the window size. However, the effect of window shift on resolution was not investigated. Cohn *et al.* [5] have also evaluated the step response for a high contrast object and then deconvolved it with a step function to get a "system strain impulse response." The accuracy of this approach may vary with target contrast because strain and modulus are nonlinearly related [6], [7] and because this approach uses linear systems analysis. "System strain impulse response" can be computed alternatively by computing the first derivative of step response. They also proposed using the autocorrelation function (ACF) of the difference between the displacement and a third-order fit to the displacement. However, no justification was given as to why this parameter may be an indicator of elastographic resolution. No attempt has been made in either approach to relate resolution to any system or processing parameter. We have proposed a modulation transfer function (MTF) approach [8] to resolution in an earlier work [9] in which resolution was defined in terms of the ability of the strain estimators to follow the cyclic strains as the rate of change of strain increases. When the estimated strain lags behind the true strain by a predetermined amount, the limit of resolution is reached according to this definition.

It is very difficult to obtain a theoretical expression for the resolution R in terms of T and Δt. In this paper, we report on the axial resolution using a simulation experiment. We have simulated a 1-D wedge-shaped phantom. We concentrate on low contrast resolution (a contrast of two is used) because resolution generally improves at high contrast [4]. Elastographic resolution may also depend on many system parameters such as the center frequency and bandwidth. Our experimental set-up typically uses a 5-MHz ultrasonic transducer with 60% fractional bandwidth. In this study, the system parameters are kept constant at these values to keep the dimensionality of the problem small.

It must be stressed that none of the resolution criteria discussed above measures the absolute limit of resolution. These criteria are only approximate treatments and are useful for comparing one system with another. A complete treatment needs to also include an analysis of the noise characteristics, which are the ultimate resolution limiting factors [10]. Because window size affects elastographic noise, a resolution study in which noise analysis is included may show a stronger dependence on the window size than we observed in this work. Additional studies could be performed to include an analysis of the noise characteristics and, separately, to evaluate the effect of systems parameters, etc.

II. Methods

A. The Wedge Phantom

We have simulated a phantom using MATLAB[1] containing a stiffer wedge-shaped inclusion in an otherwise homogeneous

Manuscript received June 2, 1998; accepted September 21, 1999. This work was supported in part by NIH grant P01-CA64597 to the University of Texas.

S. K. Alam is currently with Riverside Research Institute, New York, NY 10036 (e-mail: kalam@rrinyc.org).

J. Ophir and T. Varghese are with the Ultrasonics Laboratory, Radiology Department, The University of Texas Medical School, Houston, TX 77030.

[1]MATLAB is a registered trademark of The MathWorks, Inc. (Natick, MA).

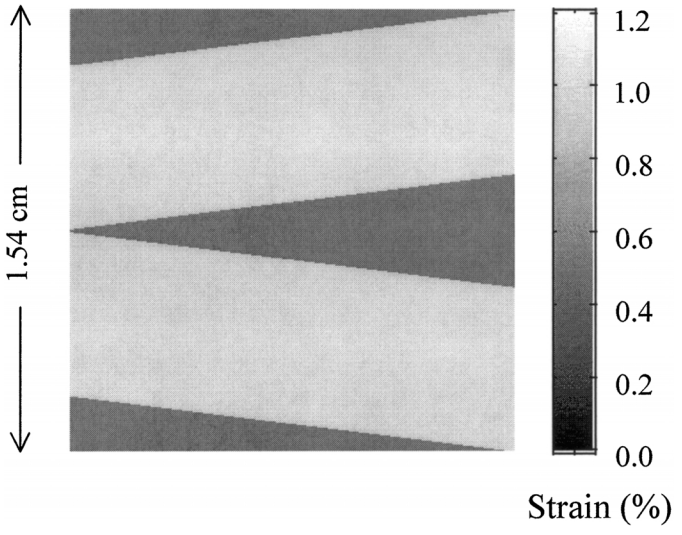

Fig. 1. Wedge phantom used in the experiment.

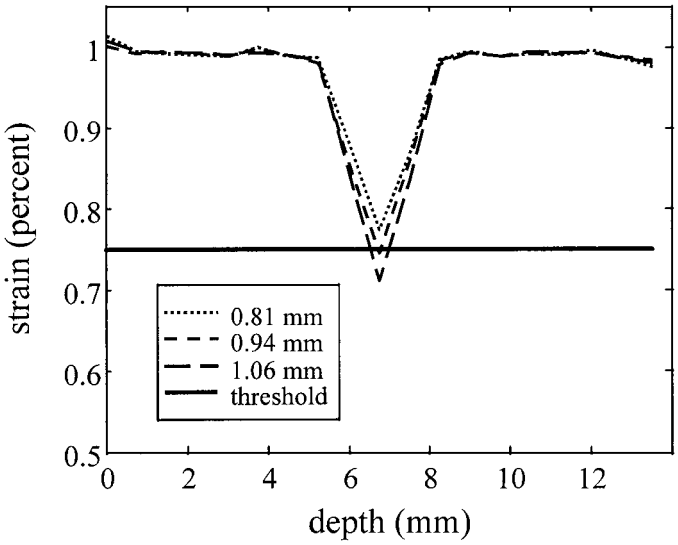

Fig. 2. Illustration of the resolution estimation.

medium. A hard inclusion was chosen because cancerous lesions are frequently stiffer than the host tissue [11]. An experimental wedge phantom has previously been used in elastography; however, it was not used quantitatively to evaluate resolution [1]. The shape of the phantom used in this study is similar to the SUAR[2] wedge phantom used to determine ultrasonic resolution using a similar principle [12]. The elastographic phantom used in this study is shown as a grayscale image in Fig. 1. The background is softer (strain = 1%), and the wedge-shaped inclusion at the middle is stiffer (strain = 0.5%). For strain estimation, we used the gradient method in conjunction with global stretching [13]. To keep the total displacement constant at every A-line, half wedges (strain = 0.5%) at the top and bottom of the phantom are included.

We used 77 lines of uniformly spaced, Gaussian-distributed random amplitude scatterers within a thin pencil beam (10 scatterers per wavelength). A total of 25 independent renditions of the wedge phantom was simulated. The Gaussian round-trip transfer function had a center frequency of 5 MHz and a noise equivalent bandwidth [14] of 60%. The signals were sampled at 50 MHz. The RF A-lines were computed by convolving the scatterer profile with the impulse response of the system. Tissue compression was simulated by appropriately time-shifting the scatterers, which was implemented using a frequency domain phase-shift algorithm. Nonaxial motion was excluded to isolate axial resolution from other effects. No attenuation was simulated.

B. Estimating the Resolution

The ability to replicate the discontinuity (notch) in strain with a predefined fidelity is used as the resolution criterion; the ability to create a notch that is at least halfway down between the top and bottom of the well was chosen. Resolution is estimated as follows: 1) compute the estimated strain profiles corresponding to each A-line; 2) define resolution as the smallest of the widths of the wedge for which the estimated strain profile drops below the midpoint (0.75%) of the high (1%) and low (0.5%) strains; 3) repeat steps 1 and 2 for 24 other independent renditions of the wedge; and 4) compute the mean and standard deviations of the computed resolutions for the 25 renditions. These four steps are repeated for a range of values of T and Δt. In computing the strain profile in step 1, the gradient method with global uniform stretching is used [9], [13], [15]. Step 2 is illustrated for a wedge with a finite step size of 0.13 mm in Fig. 2. We show the estimated strain profiles for widths of 0.81, 0.94, and 1.06 mm. The strain profile corresponding to the 0.81-mm width is above the midpoint of 0.75%, but the other two are below this threshold. (0.94 mm is the smaller of the two.) Thus, according to our definition, the estimated resolution is 0.94 mm. Note that the resolution estimates will have a finite precision because of the discrete increment of wedge step size. In actual experiments, the precision of the resolution estimate (wedge step size) of 0.03 mm was satisfactory because the resolution is generally in the millimeter range.

Finally, we fit the resolution measurements to a plane surface with the form

$$R = a_0 + a_1 T + a_2 \Delta t \tag{1}$$

where R is the resolution, T is the correlation window size, and Δt is the window shift. We chose this form because of its simplicity. We will compute the coefficient of determination r^2 to assess the goodness-of-fit. If the fit is poor ($r^2 < 0.9$), some higher order terms and some cross terms of T and Δt may need to be included. We derived the formula to be used for the least-square fit to the form in (1) following the formulation (for least-squares fit to a straight line) by Bevington and Robinson [16]. The expression used is shown in the Appendix.

III. Results

We have generated resolution values using window sizes ranging from $\frac{1}{2}$ to 4 mm, and window shifts in the range of $\frac{1}{64}$ to 2 mm. However, window shifts larger than the window sizes have not been used because then there will be unused data segments between the correlation windows. We further illustrate resolution estimation in Fig. 3 through 6. In Fig. 3, we

[2]The axial resolution wedge consisted of a water-filled wedge. Both "barely resolved" and "clearly resolved" criteria were used to determine the axial ultrasonic resolution.

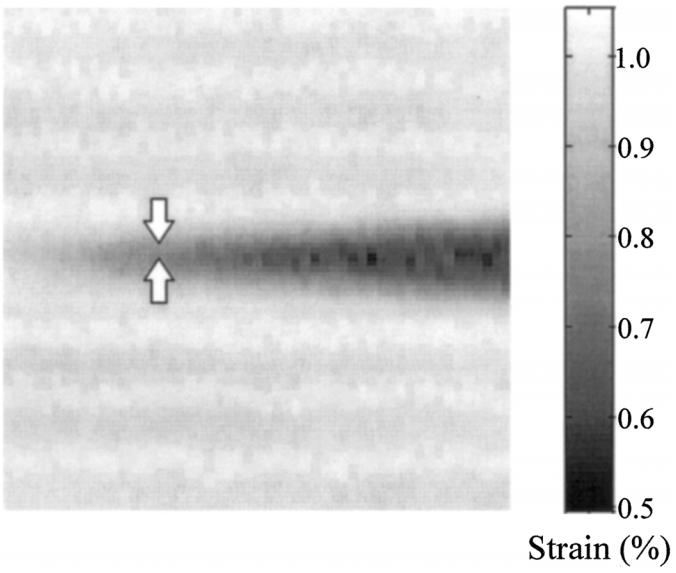

Fig. 3. Another illustration of the resolution estimation. Window size = 3 mm and window shift = 0.125 mm. The estimated resolution is 0.58 mm.

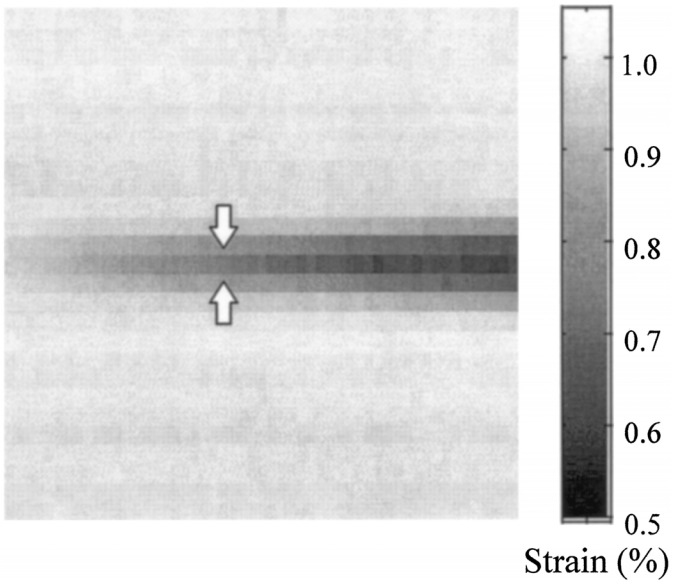

Fig. 4. Window size = 3 mm and window shift = 0.50 mm. The estimated resolution is 0.80 mm.

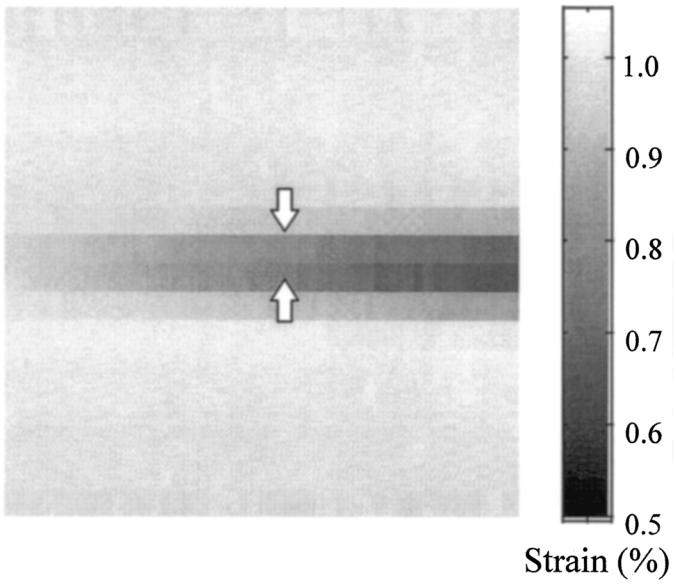

Fig. 5. Window size = 3 mm and window shift = 0.75 mm. The estimated resolution is 1.06 mm.

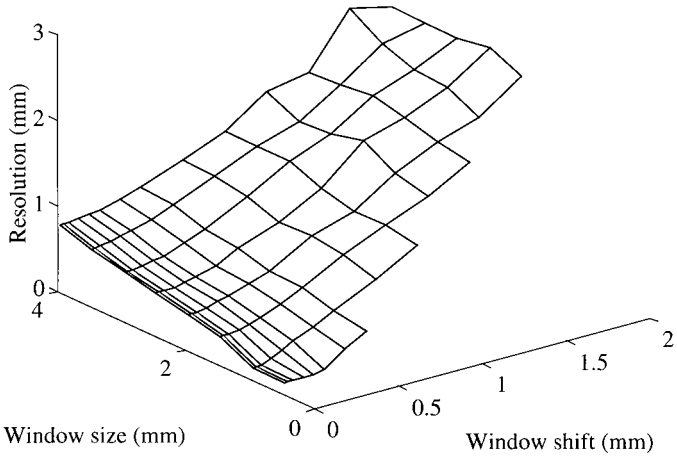

Fig. 6. Surface plot of the estimated resolution versus window size and window shift.

show the elastogram for a window size of 3 mm and window shift of 0.125 mm. The estimated resolution is 0.58 mm. The vertical arrows approximately show the A-line where the resolution criterion was satisfied and the estimated resolution itself. Fig. 4 and 5 show elastograms for a window size of 3 mm, and window shifts of 0.5 and 0.75 mm, respectively. As the window shift increases, the resolution criterion is satisfied at a thicker portion of the wedge. The estimated resolutions are 0.80 and 1.06 mm, respectively. A systematic error is observed in the elastograms, especially at smaller window sizes. These errors may be from the correlated noise in displacement estimates.

We plot estimated resolutions in Fig. 6 through 9. We plot resolution versus window size and window shift as a 2-D mesh in Fig. 6. Clearly, the window shift has a much more significant effect on the resolution compared with window size. To illustrate their comparative effects, we also plot subsets of the data versus window shift in Fig. 7 and versus window size in Fig. 8. In Fig. 7, resolution changes almost at the same rate as window shift, and the graphs for window sizes of 1.5 and 2.0 mm are very close. On the other hand, in Fig. 8, resolution changes much slower with the changes in window size, and the graphs are quite far apart for window shifts of 0.25 and 0.5 mm. However, the trend is significant in both cases in comparison with the error bars.

We have used (A.2) to fit these data to a plane surface. For the fit, we have discarded the data for $\Delta t < 0.0625$ mm because the resolution values remain virtually unchanged below this value and, thus, is not a part of the $(T, \Delta t)$ plane surface. The equation of the fit is as follows:

$$R = -0.0498 + 0.1586T + 0.8982\Delta t \tag{2}$$

with $r^2 = 0.988$. Such a large value of r^2 signifies that the fit is excellent, and the bilinear equation is sufficient to describe the

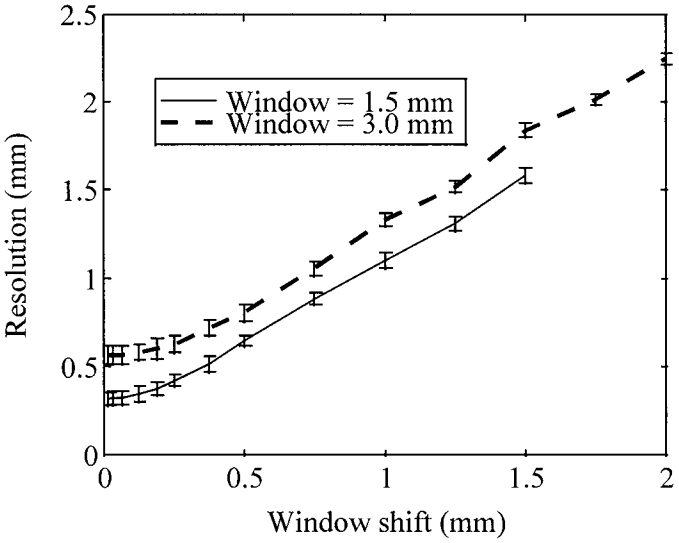

Fig. 7. Effect of window shift on resolution.

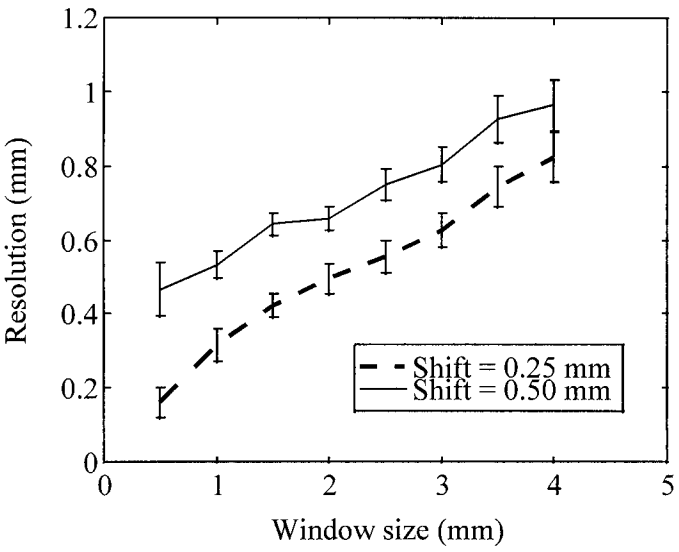

Fig. 8. Effect of window size on resolution.

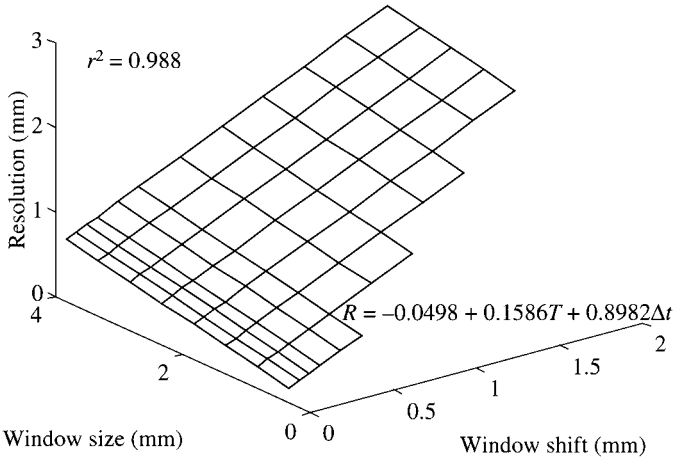

Fig. 9. Surface plot of the bilinear fit to the estimated resolution versus window size and window shift.

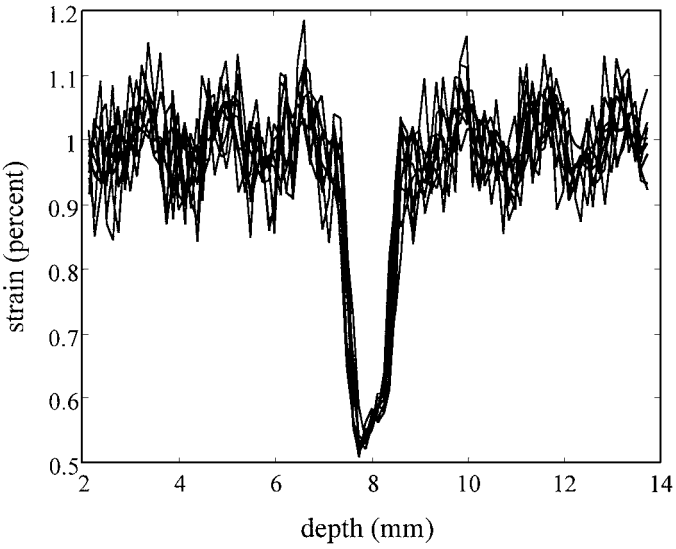

Fig. 10. Mean strain profiles corresponding to several A-lines. Window size = 0.5 mm. Window shift = 0.125 mm.

resolution. The intercept has a negative value. However, (2) is not valid for arbitrarily small values of T and Δt as is evident from the flat portion of the plot in Fig. 6 at small values of T and Δt. In Fig. 9, we display the surface plot of the fit for the range of data used in the fit ($0.5 \leq T \leq 4$, $0.0625 \leq \Delta t \leq 2$, $\Delta t \leq T$; all units in millimeters).

IV. Discussion

We have defined elastographic resolution in this paper using a controlled simulation experiment with a 1-D wedge phantom. After computing the resolution for a set of window sizes and window shifts using the defined criteria, we fit a plane surface (bilinear equation of T and Δt) through the data. We got an excellent fit ($r^2 = 0.988$). Thus, the bilinear fit is adequate, and no higher order or cross terms are necessary.

The coefficients to Δt and T are both positive as expected. (Resolution is expected to improve when either T or Δt is reduced.) Interestingly, the coefficient a_2 (to Δt) is very close to unity, and the coefficient a_1 (to T) is very close to zero. Thus, $R = -0.0498 + 0.1586T + 0.8982\Delta t \approx \Delta t$. However, the effect of the window size, although much smaller than that of the window shift, cannot be completely neglected ($a_1 \neq 0$). On the other hand, the most significant effect of increasing window size is in the reduction of the noise in the elastograms. We have plotted the mean strain profiles (at a few A-lines only) for window sizes of 0.5 and 3 mm (window shift = 0.125 mm) in Fig. 10 and 11, respectively. Clearly, the noise is significantly lower at the larger window size (Fig. 11).

This study is valid for a single center frequency (5 MHz) and bandwidth (60%) typical for our experimental set-up. Many variables affect axial resolution including contrast, signal-to-noise ratio (SNR), center frequency, bandwidth, beam size, depth, nonaxial motion, etc. However, had we attempted to include all phenomena, confounding effects would have complicated the problem and made it nearly intractable. So, we decided to separate the variables. This work can be considered the "best case" scenario. Additional studies can be performed

$$\mathbf{M} = \begin{bmatrix} \sum_i \sum_j 1 & \sum_i \sum_j x_i & \sum_i \sum_j y_j \\ \sum_i \sum_j x_i & \sum_i \sum_j x_i^2 & \sum_i \sum_j x_i y_j \\ \sum_i \sum_j y_j & \sum_i \sum_j x_i y_j & \sum_i \sum_j y_j^2 \end{bmatrix} \text{ and } \mathbf{n} = \begin{bmatrix} \sum_i \sum_j z_{i,j} \\ \sum_i \sum_j x_i z_{i,j} \\ \sum_i \sum_j y_j z_{i,j} \end{bmatrix} \tag{A.3}$$

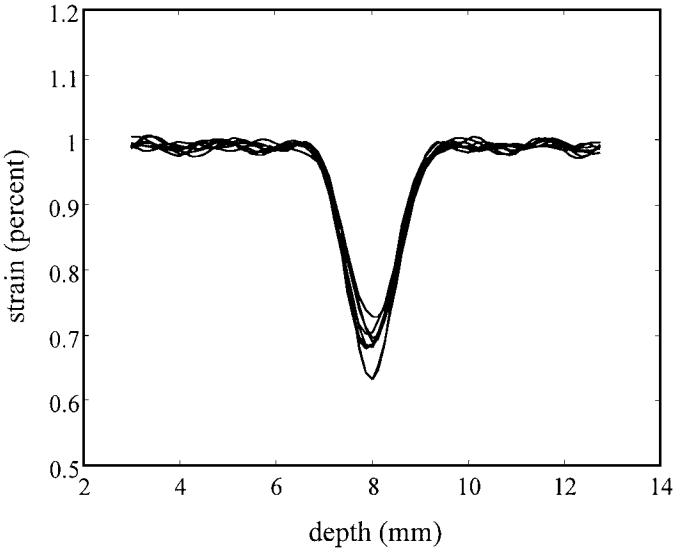

Fig. 11. Window size = 3 mm. Window shift = 0.125 mm. Compared with Fig. 11, the noise has been significantly reduced.

to evaluate the effect of changes in the system parameters. We have, in fact, shown a trade-off among center frequency, bandwidth, SNR, and resolution in a strain filter [17] formulation, and a 3-D strain filter (SNR_e versus strain and resolution) was drawn [3]. Here, window size was used as resolution. It is possible to redraw the 3-D strain filter using (2) as resolution instead of the window size.

The ultrasonic resolution for the simulated ultrasound system was on the order of 0.5 mm. The elastographic resolution that we have computed depends on the window size and the window shift and was computed to be as low as 0.125 mm and as high as >2 mm. For the window sizes and window shifts that are typically used in elastography, the elastographic resolution was found to be of the order of the sonographic resolution.

The resolution of any convolution-based imaging system such as ultrasonic imaging is ultimately diffraction-limited. Elastographic resolution improves when T and Δt are reduced. But, there is a limit to improving the elastographic resolution by making T and Δt arbitrarily small. Validity of (2) is known only for the ranges of values used in the fit ($0.5 \leq T \leq 4$, $0.0625 \leq \Delta t \leq 2$, $\Delta t \leq T$; all units in millimeters). Moreover, if we examine Fig. 6 and 7 (especially, Fig. 6) closely, we notice that, as Δt is reduced, resolution asymptotically flattens out as $\Delta t \to 0$. It is likely to be due to the fact that resolution is ultimately limited by a complex interaction of T, Δt, and the impulse response of the system. A closer look at Fig. 6 reveals that the onset of this effect is dependent on the values of T and happens at larger values of Δt when T is smaller. A more complete study can be conducted to determine the dependence of the resolution limit on the impulse response of the ultrasound system.

Eq. (2) is strictly valid for the gradient strain estimator in conjunction with global uniform stretching [13]. If global stretching is not used for the gradient strain estimation, then the elastograms will be noisier. However, the resolution estimates may not be very different, although some variation is expected because of the increased noise itself. The results will likely be different if some other estimator, such as a least squares [18] or adaptive stretching [9], is used. In adaptive stretching, window shift is expected to have a much smaller effect on resolution. The windowed postcompression A-line segment is stretched iteratively in adaptive stretching until the correlation between this and the corresponding precompression segment maximizes (the stretch factor itself is used to compute strain); thus, only intrawindow operations are necessary. As a result, when the data window is completely within the notch, the expected value of estimated strain will not be affected by other surrounding strains and equal the strain in the notch. Gradient methods, on the other hand, compute strains from the first difference of the displacement estimates. Thus, even when a data window is completely inside the notch, the strain estimate at that location will be influenced by the displacement estimates at the neighboring data windows that may be outside the notch.

The results will also be different if we chose a different criterion for computing resolution. In this study, we did not include an ultrasonic beam. Inclusion of the beam (or changing the beam size) is very likely to change (2) even if we do not change the criterion. If a different type of target is used, or if psychovisual experiments are performed instead of the objective measure used in this paper, the definition of resolution will likely change also. Nevertheless, we believe that the trend that we have observed in this paper will not change significantly.

Because the entire elastographic process is nonstationary [19], [20], the resolution is also nonstationary. The point-spread function (PSF) varies with depth: 1) frequency-dependent attenuation and scattering reduces the center frequency with depth, and 2) the ultrasonic pulse elongates in front of the focus because of the varying arrival time from various sections of the transducer, resulting in reduced bandwidth. When tissue is compressed, it undergoes a 3-D motion. But, the nonaxial motion has been ignored in elastography until recently. Some recent papers have investigated these issues and reported successful reduction of degradation because of nonaxial motion. Accounting for other effects will degrade the resolution and will be undertaken in future work. Thus, the results that we have presented in this paper can be considered as the best case scenario or the axial resolution at the focus of the transducer.

In an earlier paper [9], we described an MTF approach [8] that may be useful in estimating resolution. However, the only approach that worked so far to follow adequately the rapid variations in strain was adaptive stretching [9]. In another work in which resolution was used interchangeably with window size [3], the window shift was kept at a constant percentage of window size ($\Delta t/T$ = constant); thus, Δt was indirectly changed.

Because $R \approx t$, any plot versus resolution was off by a constant factor.

Céspedes [4] has shown that very thin soft targets can be detected with elastography. Soft targets undergo larger strains that contribute to larger decorrelations. It was shown that paper-thin soft layers (20 times softer) are visible in elastograms because of the noisy strain estimates around the soft area caused by large decorrelation. But, similar thickness hard layers (20 times harder) are not visible. This motivated us not to use simple detection as a resolution criterion but to use the ability of replicate the strain profile within a predefined error.

Acknowledgments

The authors gratefully acknowledge the helpful comments from the anonymous reviewers and thank Dr. Mike Insana of the University of Kansas for fruitful discussions. This work was performed at University of Texas.

Appendix

A. Least-Squares Fit to a Plain Surface

We want to fit a plain surface through some 3-D data points. Many textbooks address fitting a straight line through 2-D data. However, expression for fitting a plane surface through 3-D data are not commonly available. If the functional relationship between the dependent (z) and independent (x, y) variables is approximated by

$$z(x, y) = a + bx + cy, \tag{A.1}$$

then, for an observation set of x_i,y_j, and $z_{i,j}$, the least-squares fit to a plane surface can be expressed in the following matrix form:

$$\begin{bmatrix} a \\ b \\ c \end{bmatrix} = \mathbf{M^{-1}n} \tag{A.2}$$

where [see (A.3), top of previous page].

References

[1] J. Ophir, I. Céspedes, H. Ponnekanti, Y. Yazdi, and X. Li, "Elastography: A method for imaging the elasticity in biological tissues," *Ultrason. Imag.*, vol. 13, pp. 111–134, 1991.

[2] W. F. Walker and G. E. Trahey, "A fundamental limit on the performance of correlation based phase correction and flow estimation techniques," *IEEE Trans. Ultrason., Ferroelect., Freq. Contr.*, vol. 41, pp. 644–654, 1994.

[3] T. Varghese, M. Bilgen, and J. Ophir, "Multiresolution imaging in elastography," *IEEE Trans. Ultrason., Ferroelect., Freq. Contr.*, vol. 45, pp. 65–75, 1998.

[4] I. Céspedes, "Elastography: Imaging of biological tissue elasticity," Ph.D. dissertation, University of Houston, Texas, 1993.

[5] N. A. Cohn, S. Y. Emelianov, and M. O'Donnell, "An elasticity microscope. Part II: Experimental results," *IEEE Trans. Ultrason., Ferroelect., Freq. Contr.*, vol. 44, pp. 1320–1331, 1997.

[6] H. Ponnekanti, J. Ophir, Y. Huang, and I. Céspedes, "Fundamental mechanical limitations on the visualization of elasticity contrast in elastography," *Ultrason. Med. Biol.*, vol. 21, pp. 533–543, 1995.

[7] F. Kallel, M. Bertrand, and J. Ophir, "Fundamental limitations on the contrast-transfer efficiency in elastography: An analytic study," *Ultrason. Med. Biol.*, vol. 22, pp. 463–470, 1996.

[8] J. W. Goodman, *Introduction to Fourier Optics*. New York: McGraw-Hill, 1968.

[9] S. K. Alam, J. Ophir, and E. E. Konofagou, "An adaptive strain estimator for elastography," *IEEE Trans. Ultrason., Ferroelect., Freq. Contr.*, vol. 45, pp. 461–472, 1998.

[10] G. O. Reynolds, J. B. DeVelis, G. B. Parrent, Jr., and B. J. Thompson, *The New Physical Optics Notebook: Tutorials in Fourier Optics*. Bellingham, WA: SPIE and New York, NY: American Institute of Physics, 1989.

[11] T. A. Krouskop, T. W. Wheeler, F. Kallel, B. S. Garra, and T. Hall, "Elastic moduli of breast and prostate tissues under compression," *Ultrason. Imag.*, vol. 20, pp. 260–274, 1998.

[12] P. L. Carson and J. A. Zagzebski, "Pulse echo ultrasound imaging systems: Performance tests and criteria," AAPM Rep. #8, Library of Congress No. 81-66437. Amer. Assoc. Physicists Med., College Park, MD, pp. 51, 1981.

[13] I. Céspedes and J. Ophir, "Reduction of image noise in elastography," *Ultrason. Imag.*, vol. 15, pp. 89–102, 1993.

[14] J. S. Bendat and A. C. Piersol, *Random Data: Analysis and Measurement Procedures*, 2nd Ed. New York: John Wiley and Sons, 1986.

[15] S. K. Alam and J. Ophir, "Reduction of signal decorrelation from mechanical compression of tissues by temporal stretching—applications to elastography," *Ultrason. Med. Biol.*, vol. 23, pp. 95–105, 1997.

[16] P. R. Bevington and D. K. Robinson, *Data Reduction and Error Analysis for the Physical Sciences*, 2nd Ed. New York: McGraw-Hill, 1992.

[17] T. Varghese and J. Ophir, "A theoretical framework for performance characterization of elastography: The strain filter," *IEEE Trans. Ultrason., Ferroelect., Freq. Contr.*, vol. 44, pp. 164–172, 1997.

[18] F. Kallel and J. Ophir, "A least squares estimator for elastography," *Ultrason. Imag.*, vol. 19, pp. 195–208, 1997.

[19] T. Varghese and J. Ophir, "The nonstationary strain filter in elastography. Part I. Frequency dependent attenuation," *Ultrason. Med. Biol.*, vol. 23, pp. 1343–1356, 1997.

[20] F. Kallel, T. Varghese, J. Ophir, and M. Bilgen, "The nonstationary strain filter in elastography. Part II. Lateral and elevational decorrelation," *Ultrason. Med. Biol.*, vol. 23, pp. 1357–1369, 1997.